Comprehensive analysis of high-lying states in ^{18}O populated with (t,p) and $(^{18}O,^{16}O)$ reactions

M. J. Ermamatov,[1,2] R. Linares,[1] J. Lubian,[1] J. L. Ferreira,[1] F. Cappuzzello,[3,4] D. Carbone,[3] M. Cavallaro,[3] M. Cubero,[5] P. N. de Faria,[1] A. Foti,[3,4] G. Santagati,[3] and V. A. B. Zagatto[1]

[1]*Instituto de Física, Universidade Federal Fluminense, 24210-340 Niterói, Brazil*
[2]*Institute of Nuclear Physics, Ulughbek, Tashkent 100214, Uzbekistan*
[3]*INFN, Laboratori Nazionali del Sud, I-95125 Catania, Italy*
[4]*Dipatimento di Fisica e Astronomia, Università di Catania, I-95125 Catania, Italy*
[5]*CICANUM, Universidad de Costa Rica, 11502 Apartado, 2060 San José, Costa Rica*

(Received 24 July 2017; published 4 October 2017)

Background: In our recent work [M. J. Ermamatov *et al.*, Phys. Rev. C **94**, 024610 (2016)], the two-neutron transfer induced by the (^{18}O,^{16}O) reaction was studied for ^{16}O nucleus. Theoretical analysis of the low-lying states of ^{18}O indicates that the transfer to the ground state proceeds predominantly through simultaneous transfer of the two-neutron system.

Purpose: In this work, we extend our previous theoretical analysis towards high-lying states of the ^{18}O nucleus. In order to achieve a comprehensive picture, we revisit the experimental data for the ^{16}O$(t,p)^{18}$O reaction at 15 MeV bombarding energy. We also include new experimental cross sections for the high-lying states of the ^{18}O residual nucleus, populated in the ^{16}O(^{18}O,^{16}O)^{18}O reaction at 84 MeV.

Method: The same spectroscopic parameters of the target nucleus were used as input in the coupled channel calculations for the transfer induced by triton and ^{18}O projectiles. Simultaneous two-neutron transfer is calculated within the coupled reaction channel approach, using the extreme cluster and independent coordinate models. The sequential process is calculated within the distorted-wave Born approximation.

Results: Theoretical calculations reproduce the ^{16}O$(t,p)^{18}$O data well, leading to natural parity states in the ^{18}O nucleus without the need of adjustable parameters. The same methods are applied to the ^{16}O(^{18}O,^{16}O)^{18}O data and a good agreement is observed.

Conclusions: Detailed analyses show the importance of a simultaneous mechanism for the two-neutron transfer reactions. In transferring two neutrons, the pairing correlation plays an important role.

DOI: 10.1103/PhysRevC.96.044603

I. INTRODUCTION

Transfer reactions are long-standing tool for obtaining detailed information on the nuclear wave functions. In the past, intensive research has been carried out exploiting reactions induced by proton, deuteron, and triton beams. The (t,p) and (p,t) reactions provide complementary information to the (p,d) or (d,p) ones. For instance, the one-neutron stripping or pick-up reactions led to a complete determination of the wave function of the 0^+ ground state (g.s.) in the ^{18}O nucleus in terms of a linear combination of $(1d_{5/2})^2$, $(2s_{1/2})^2$, and collective states. For the 0^+_2(3.63 MeV) and 0^+_3 (5.33 MeV) states, the data allowed two different sets of solutions [1]. This ambiguity is completely removed under the light of the experimental data provided by the ^{16}O(t,p) reaction, in which dominance of the $(s_{1/2})^2$ component for the 0^+_3 state has been shown [1].

The (t,p) probe has the advantage that the neutron-neutron singlet correlation (pairing) has a role in the mean field, while other degrees of freedom (like the relative motion of the two neutrons with respect to the proton) are treatable. Nevertheless, a full description of the two-nucleon transfer processes requires a detailed four-body approach due to the mutual interactions between the two cores (of the projectile and the target nuclei) and the two nucleons [2]. The complexity of such four-body scattering is usually reduced to the direct nuclear reaction formalism in which simultaneous (t-p) and sequential (t-d-p) two-nucleon transfers are independently calculated. For the simultaneous process, analyses of (p,t) and (t,p) reactions have been carried out within the distorted-wave Born approximation (DWBA) [1,3]. The sequential process is usually calculated within the second-order DWBA [4]. Recently, a method of calculation that considers the contributions from simultaneous and sequential transfers has been developed and compared with the (t,p) and (p,t) reactions with Sn isotopes [5,6]. In such a method, the nonorthogonality term, that arises from couplings between different mass partitions, is properly treated.

Nucleon transfers induced by heavy-ion projectiles have been less exploited due to experimental and theoretical complexities. Such reactions are typically characterized by the high angular momenta in the entrance and exit channels, that imposes difficulties for a numerical convergence, since many partial waves are needed in the direct reaction calculations. Moreover, inelastic channel couplings cannot be neglected. On the other hand, beams of heavy-ion projectiles can be accelerated with sufficiently high intensity to allow small cross sections of the two-neutron transfer reactions to be studied effectively. In addition, the transfer probability to a specific set of states in the residual nuclei can be tuned based on the Q-matching kinematics [7].

In the systematic study of one- and two-neutron excitations [8–11], the feasibility of spectroscopic studies in the transfer reactions induced by ^{18}O projectiles has been demonstrated for light and medium mass nuclei. The theoretical approach

consists of coupled reaction channel (CRC) and DWBA calculations with relevant channels included. Spectroscopic amplitudes have been obtained from shell model calculations. Within this framework, and without the need of scaling factors, we have successfully reproduced the experimental angular distributions for the two-neutron transfer to ^{12}C [9], ^{13}C [12], and ^{16}O [13] leading to the 0^+_1 and 2^+_1 natural parity states of residual nuclei. In such studies, we demonstrated the predominance of simultaneous (direct) transfer over sequential transfer in these systems, in agreement with the conclusions obtained with the (t,p) reaction to the low-lying states.

A comparison of the two-neutron results to high-lying states, deduced from heavy-ion and light-ion reactions, is still lacking. Incorporating bound states at high excitation energies into the direct reaction calculations is challenging from the computational point of view. The resonant states of ^{10}Be, populated via the ^{9}Be(^{18}O,^{17}O) reaction, and ^{15}C, populated via the ^{13}C(^{18}O,^{16}O) reaction [8,11], have been studied in the light of semiclassical models. These exploratory analyses highlighted the effect of the neutron-core configuration on the properties of such resonant states.

This work revisits the two-neutron transfer to ^{16}O induced by the (t,p) [14] and (^{18}O,^{16}O) [13] reactions, aiming at a consistent description of the experimental cross sections leading to the population of high-lying states in ^{18}O nucleus. Experimental data for the ^{16}O$(t,p)^{18}$O reaction at 15 MeV (beam energy) consist of angular distributions for the states up to 7.1 MeV excitation energy in ^{18}O. We also include new experimental data from the ^{16}O(^{18}O,^{16}O)^{18}O reaction at 84 MeV for states up to 9.1 MeV.

The paper is organized as follows: in Sec. II we present the experimental details; in Sec. III experimental data on ^{16}O(t,p)^{18}O are analyzed, comparing them with the theoretical calculations; and in Sec. IV new experimental data on ^{16}O(^{18}O,^{16}O)^{18}O reaction are analyzed within the same approaches. Concluding remarks are given in Sec. V.

II. THE EXPERIMENTAL DATA

A. The ^{16}O$(t,p)^{18}$O data

The experimental data on the ^{16}O$(t,p)^{18}$O reaction have been reported in Ref. [14]. A triton beam was accelerated at 15 MeV towards a gas cell containing isotopically enriched ^{16}O gas. Outgoing protons were momentum analyzed by a spectrograph and detected in emulsion plates. The angular distributions of the absolute cross-sections up to the 4^+_2 state (at 7.13 MeV) were measured with 10% accuracy.

The spectrum shown in Fig. 1 of Ref. [14] indicates an energy resolution, defined as the full width half maximum (FWHM), of about 20 keV. Moreover, the only observed contaminant comes from the hydrogen present in the target, producing a wide structure at energies between 8.9 and 9.1 MeV in ^{18}O excitation energy.

B. The ^{16}O(^{18}O,^{16}O)^{18}O data

The reaction was performed at the Istituto Nazionale di Fisica Nucleare–Laboratori Nazionali del Sud, Catania, Italy, using an 84 MeV ^{18}O beam accelerated towards a WO_3 target

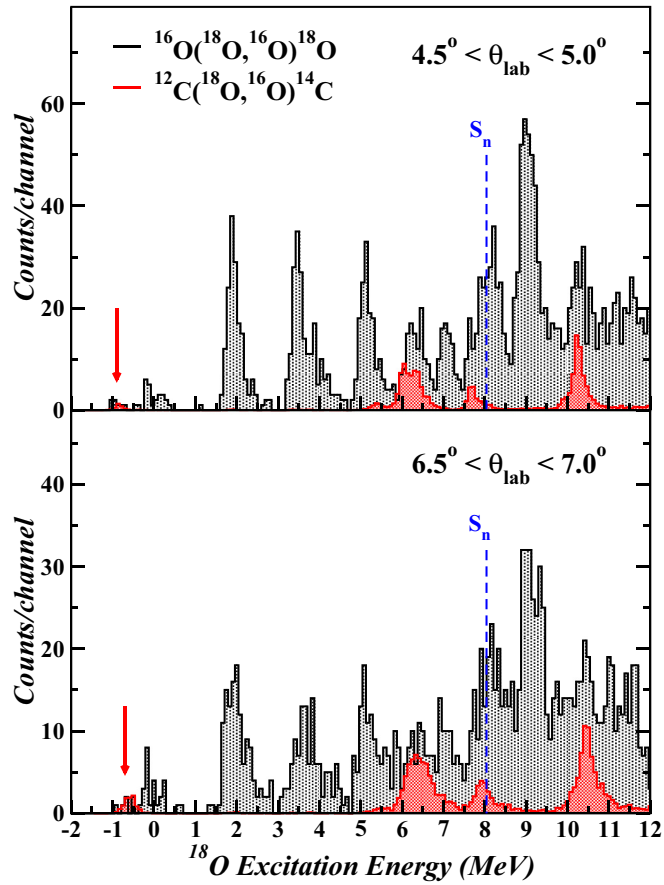

FIG. 1. Excitation energy spectra of ^{18}O populated with the ^{16}O(^{18}O,^{16}O)^{18}O reaction (black histograms) at two angular ranges: $4.5^\circ < \theta_{lab} < 5.0^\circ$ (a) and $6.5^\circ < \theta_{lab} < 7.0^\circ$ (b). The red histograms represent the background arising from the ^{12}C backing in the WO_3 target. An arbitrary factor is applied to the red histogram to make easier the comparison with the full histogram. The energy threshold for neutron emission (S_n) is indicated by the dashed blue line. The red arrows point at the peaks associated with the g.s. → g.s. two-neutron transfer to the ^{12}C nucleus, adopted to estimate the proper normalization factor for the background substraction. Energy bin size is approximately 83 keV.

(212 μg/cm^2 thickness). Ejectiles from the reaction were momentum analyzed by the MAGNEX spectrometer [15]. Details of the experimental setup are provided in Ref. [13].

The excitation energy spectra, relative to the ground-state to ground-state Q value, of the ^{16}O(^{18}O,^{16}O)^{18}O reaction, measured at $4.5^\circ < \theta_{lab} < 5.0^\circ$ and $6.5^\circ < \theta_{lab} < 7.0^\circ$, are shown in Fig. 1 (dark histograms). The energy resolution is 250 keV (FWHM) and allows for a clear identification of the ground and 2^+_1 (1.98 MeV) states. A supplementary measurement was performed using a 49 μg/cm^2 self-supporting ^{12}C target for estimating the contribution from carbon buildup on the WO_3 target. These background spectra are also presented in Fig. 1 (red histograms) with an arbitrary normalization factor for visualization purpose. For the background subtraction, the number of events in the peak associated with the g.s. → g.s. transition in the two-neutron transfer to the ^{12}C nucleus (red arrow, Fig. 1) has been adopted as a reference.

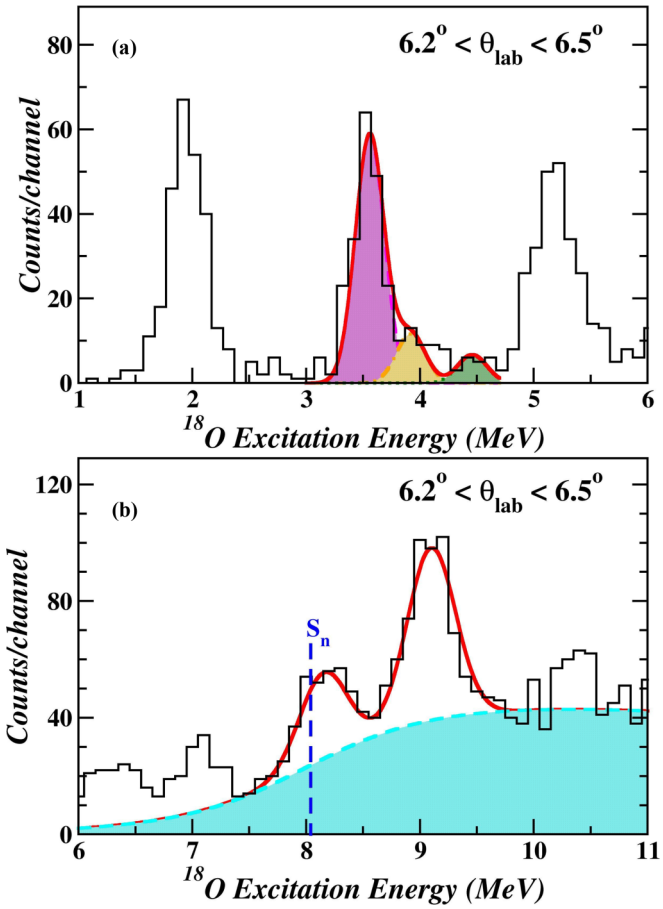

FIG. 2. Example of the fitting procedure applied to the experimental spectra. Panel (a) shows the Gaussian shapes for the 4_1^+ and 0_2^+ states (purple solid curve), the 2_2^+ state (orange solid curve), and the 1_1^- state (green solid curve). Panel (b) shows the Gaussian shapes upon a continuum background (light blue solid curve). The resonant state at ∼9.10 MeV is highly populated and exhibits a FWHM of about 0.35 MeV. The one-neutron threshold energy (S_n) is indicated by the dashed blue line.

In the previous work [13] we focused on the cross sections leading to the 0_1^+ and 2_1^+ (1.98 MeV) ^{18}O states. Determination of the cross-sections for other states requires a judicious analysis, since some states are either not fully resolved, like the 4_1^+ (3.55 MeV), 0_2^+ (3.63 MeV), and 2_2^+ (3.92 MeV) triplet states, or significantly affected by the ^{12}C impurity, like the states lying between 6.0 and 6.7 MeV in ^{18}O excitation energy. In these cases, the number of events of each angular bin was determined from the fitting, using Gaussian shapes centered at the expected excitation energies and with fixed width, according to the energy resolution. Only the amplitudes of the functions were kept free to be adjusted to the energy spectrum.

Figure 2(a) shows examples of the fitting procedure applied to the 4_1^+, 0_2^+, and 2_2^+ triplet states and the 1_1^- (4.46 MeV) state. The experimental spectrum indicates that the 4_1^+ and 0_2^+ states are more populated (purple solid curve) compared to the 2_2^+(orange solid curve). For future discussions regarding the unresolved triplet states at 3.55, 3.63, and 3.92 MeV, respectively, we extract the cross sections for the sum of these states. Above the one-neutron threshold (at 8.05 MeV), we observe a resonant state around 9.10 MeV, and approximately 0.35 MeV full width half maximum, likely corresponding to the one populated in the (t,p) reaction. The fitting procedure for this peak takes into account Gaussian shapes upon a smooth function that estimates the underlying contribution from the background continuum [see Fig. 2(b)]. Different sets of the trial function parameters (amplitude, variance, and centroid energy) that give an accurate description of the continuum background were considered and taken into account for the final estimates of the cross sections for the state on top of the background.

III. THEORETICAL FRAMEWORK

A. Direct reaction approach

Theoretical analyses of the angular distributions of the states considered for the ^{16}O$(t,p)^{18}$O reaction were performed previously in Ref. [14], within zero-range approximations to the DWBA, requiring normalization factors to describe the orders of magnitude of the angular distributions. In this way, calculations reproduced the overall shape of the angular distributions and relative magnitudes of the cross sections for transfer reactions, leading to the ground state and to many excited states in the ^{18}O nucleus. The two-neutron transfer in the ^{16}O(^{18}O,^{16}O)^{18}O reaction, leading to the population of the ground (0_1^+) and 2_1^+ states of the ^{18}O nucleus, has been analyzed in the exact finite-range CRC and two-step DWBA [13]. Results observed in (t,p) and (^{18}O,^{16}O) analysis seem to support the claim that the reaction mechanism leading to natural parity states in the even-even nucleus is dominated by the one-step simultaneous transfer process.

In a step further, we aim to achieve a comprehensive description and assess the mechanisms of two-neutron transfers (simultaneous and sequential) to the population of high-lying states in the ^{18}O nucleus. The cornerstone of this work is to employ the same theoretical method to calculate the transfer mechanism induced by (t,p) and (^{18}O,^{16}O) two-neutron transfer reactions. The approach developed in Ref. [5] is suitable whenever inelastic channels can be neglected. This is not always appropriate for reactions induced by heavy ions. In particular, there is evidence of the important role of the 2^+ state at 1.98 MeV of ^{18}O in the (^{18}O,^{16}O) reaction [16]. Therefore, here we adopt a distinct approach for simultaneous and sequential transfers.

For the simultaneous process, we employ the exact finite-range CRC (EFR-CRC) with nonorthogonality corrections and full complex remnant terms. Within the context of simultaneous transfer, we have performed calculations with the following approaches for the two-neutron system:

(1) The extreme cluster model, in which the relative motion of the two neutrons is frozen and separated from the center of mass. The wave function of the cluster with respect to the core is determined by the principal quantum number N and the orbital angular momentum L. In transforming the wave functions of the two independent nucleons in orbits n_i,ℓ_i into a cluster, the total number of quanta should be conserved according to the rule $\sum_{i=1}^{2} 2(n_i-1)+\ell_i = 2(N-1)+L$ [17].

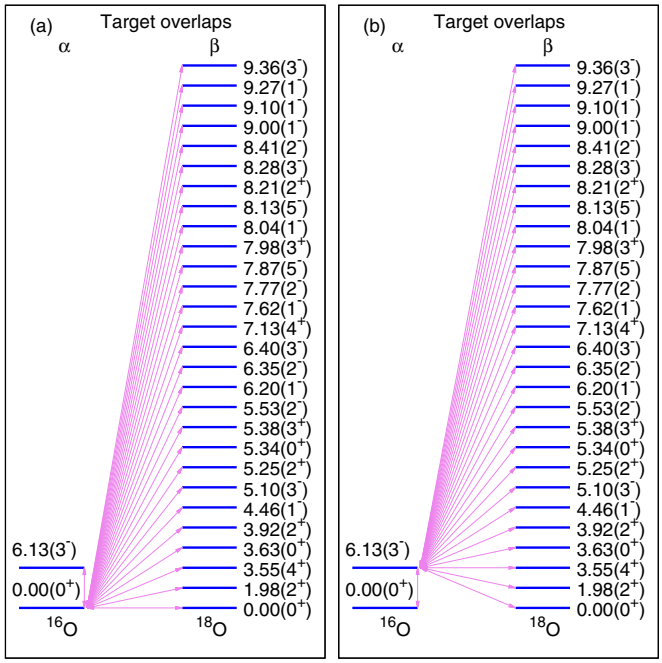

FIG. 3. Coupling for direct CRC calculations. For better visibility, the couplings of ^{16}O g.s. and 3^- excited states with the ground and excited states of ^{18}O are separated as (a) and (b), respectively.

(2) The independent coordinates (IC) model, in which the relative positions of two neutrons and two-neutron center of mass with respect to the core are considered.

Recently, we introduced the microscopic cluster model for the interpretation of the two-neutron transfer to the ^{13}C nucleus [12]. In this approach, the spectroscopic amplitudes in the center-of-mass frame of reference are derived from shell model calculations using the Moshinsky transformation brackets. According to the results of the microscopic cluster and the extreme cluster models, the unpaired neutron in the ^{13}C nucleus does not destroy the neutron-neutron correlation in the wave functions. In this work we are not considering the microscopic cluster model, since the extreme cluster model is the simplest approach and already gives a qualitative insight into the two-neutron pairing correlation in the high-lying states of the ^{18}O nucleus. In some sense, the extreme cluster and the IC models can be considered limiting approaches.

The sequential processes are treated within the coupled channel Born approximation (CCBA), taking into account inelastic excitations in the entrance partition to finite order, and adopting the two-step couplings within the DWBA method for the successive transfer of nucleons. For simplicity, herein we refer to these calculations just as two-step DWBA.

In all these calculations, we have used the São Paulo double folding potential [18] as the optical potential. In the entrance partition, a strength coefficient of 0.6 for the imaginary part of the optical potential was used to account for dissipative processes and for missing couplings to continuum states, which were not explicitly considered [19]. We use the same strength coefficient for the reaction with the triton even though this value could be smaller, since in this case not many reaction

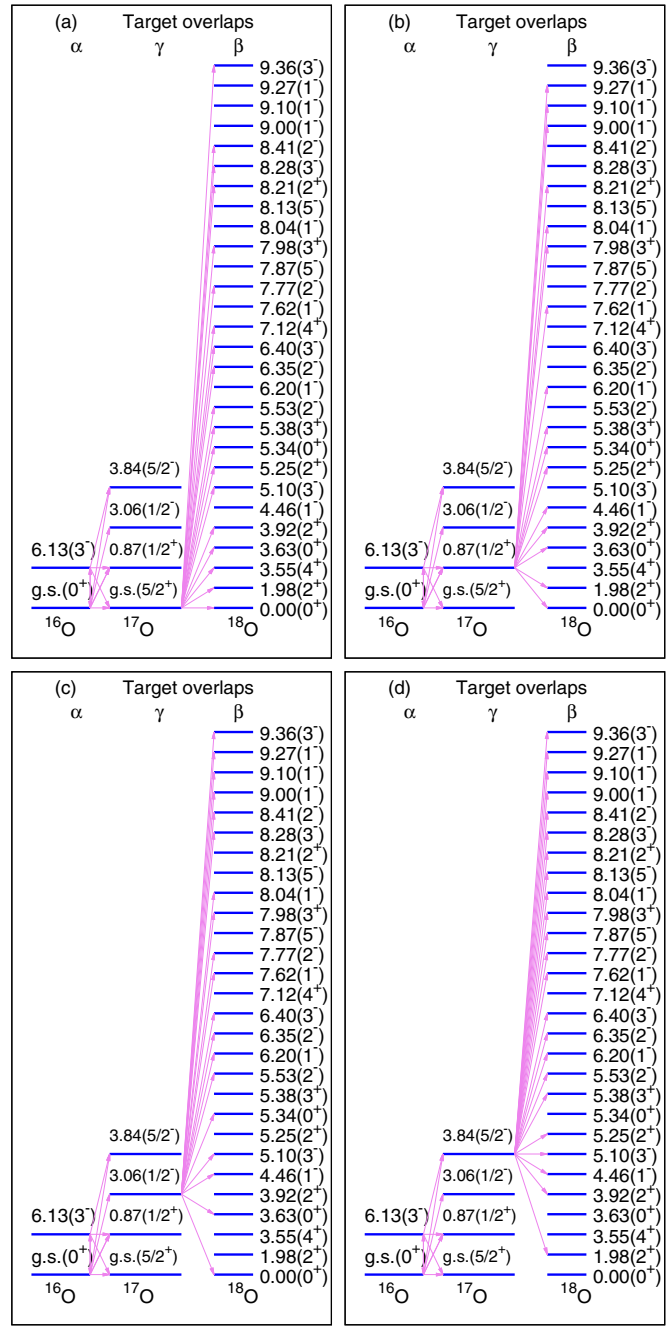

FIG. 4. Coupling for two-step DWBA calculations. For better visibility, the couplings of excited states of ^{18}O with the ^{17}O g.s. and $1/2^+$, $1/2^-$, and $5/2^-$ states are separated as (a), (b), (c), and (d), respectively.

channels are open. In the outgoing and intermediate partitions, the imaginary part was scaled by a larger factor (0.78), because no couplings were introduced. This coefficient has been proved to be suitable for describing the elastic scattering cross section for many systems in a wide energy interval [20,21]. A Woods-Saxon shape was taken to derive the form factor for the one- and two-neutron wave functions. The depth of these potentials was varied to fit the experimental separation energies in each case. The reduced radii and diffuseness were

TABLE I. One-neutron spectroscopic amplitudes (SA) for two-step DWBA calculations, obtained by shell model calculations with ZBM interaction. nl_j are the principal quantum numbers, the orbital and the total angular momenta of the single neutron.

Final state	nl_j	Initial state	SA	Final state	nl_j	Initial state	SA
$^{17}O_{g.s.}(5/2^+)$	$1d_{5/2}$	$^{18}O_{g.s.}(0^+)$	1.305	$^{17}O_{3.06}(1/2^-)$	$1p_{1/2}$	$^{18}O_{g.s.}(0^+)$	−0.929
	$2s_{1/2}$	$^{18}O_{1.98}(2^+)$	0.666		$1p_{1/2}$	$^{18}O_{3.63}(0^+)$	0.562
	$1d_{5/2}$		0.929		$2s_{1/2}$	$^{18}O_{4.46}(1^-)$	0.215
	$1d_{5/2}$	$^{18}O_{3.56}(4^+)$	1.365		$1d_{5/2}$	$^{18}O_{5.10}(3^-)$	0.233
	$1d_{5/2}$	$^{18}O_{3.63}(0^+)$	0.575		$1p_{1/2}$	$^{18}O_{5.34}(0^+)$	0.052
	$2s_{1/2}$	$^{18}O_{3.92}(2^+)$	−0.627		$1d_{5/2}$	$^{18}O_{5.53}(2^-)$	−0.206
	$1d_{5/2}$		0.987		$2s_{1/2}$	$^{18}O_{6.20}(1^-)$	0.148
	$1p_{1/2}$	$^{18}O_{5.10}(3^-)$	−0.081		$1d_{5/2}$	$^{18}O_{6.35}(2^+)$	0.404
	$2s_{1/2}$	$^{18}O_{5.25}(2^+)$	−0.348		$1d_{5/2}$	$^{18}O_{6.40}(3^-)$	0.759
	$1d_{5/2}$		−0.020		$2s_{1/2}$	$^{18}O_{7.62}(1^-)$	0.046
	$1d_{5/2}$	$^{18}O_{5.34}(0^+)$	−0.268		$1d_{5/2}$	$^{18}O_{7.77}(2^-)$	0.587
	$2s_{1/2}$	$^{18}O_{5.38}(3^+)$	0.947		$2s_{1/2}$	$^{18}O_{8.04}(1^-)$	0.630
	$1d_{5/2}$		0.003		$1d_{5/2}$	$^{18}O_{8.28}(3^-)$	−0.268
	$1p_{1/2}$	$^{18}O_{5.53}(2^-)$	−0.098		$1d_{5/2}$	$^{18}O_{8.41}(2^-)$	−0.282
	$1p_{1/2}$	$^{18}O_{6.35}(2^-)$	−0.179		$2s_{1/2}$	$^{18}O_{9.00}(1^-)$	0.100
	$1p_{1/2}$	$^{18}O_{6.40}(3^-)$	−0.319		$2s_{1/2}$	$^{18}O_{9.10}(1^-)$	0.132
	$1d_{5/2}$	$^{18}O_{7.12}(4^+)$	0.002		$2s_{1/2}$	$^{18}O_{9.27}(1^-)$	0.029
	$1p_{1/2}$	$^{18}O_{7.77}(2^-)$	−0.221		$1d_{5/2}$	$^{18}O_{9.36}(3^-)$	0.095
	$2s_{1/2}$	$^{18}O_{7.98}(3^+)$	0.261		$1p_{1/2}$	$^{18}O_{1.98}(2^+)$	0.825
	$1d_{5/2}$		−0.010		$1p_{1/2}$	$^{18}O_{3.92}(2^+)$	−0.023
	$2s_{1/2}$	$^{18}O_{8.21}(2^+)$	0.012		$1d_{5/2}$	$^{18}O_{4.46}(1^-)$	0.607
	$1d_{5/2}$		−0.010		$2s_{1/2}$	$^{18}O_{5.10}(3^-)$	−0.333
	$1p_{1/2}$	$^{18}O_{8.28}(3^-)$	0.061		$1d_{5/2}$		−0.439
	$1p_{1/2}$	$^{18}O_{8.41}(2^-)$	−0.080		$1p_{1/2}$	$^{18}O_{5.25}(2^+)$	0.092
	$1p_{1/2}$	$^{18}O_{9.27}(2^-)$	0.008		$1p_{1/2}$	$^{18}O_{5.38}(3^+)$	0.057
	$1p_{1/2}$	$^{18}O_{9.36}(3^-)$	−0.028		$2s_{1/2}$	$^{18}O_{5.53}(2^-)$	0.435
	$2s_{1/2}$	$^{18}O_{g.s.}(0^+)$	−0.561		$1d_{5/2}$		−0.743
	$1d_{5/2}$	$^{18}O_{1.98}(2^+)$	−0.652		$1d_{5/2}$	$^{18}O_{6.20}(1^-)$	0.647
	$2s_{1/2}$	$^{18}O_{3.63}(0^+)$	0.639		$2s_{1/2}$	$^{18}O_{6.35}(2^-)$	0.041
	$1d_{5/2}$	$^{18}O_{3.92}(2^+)$	0.622		$1d_{5/2}$		−0.595
	$1p_{1/2}$	$^{18}O_{4.46}(1^-)$	−0.143		$2s_{1/2}$	$^{18}O_{6.40}(3^-)$	−0.065
	$1d_{5/2}$	$^{18}O_{5.25}(2^+)$	0.326		$1d_{5/2}$		−0.200
	$2s_{1/2}$	$^{18}O_{5.34}(0^+)$	−1.085		$1d_{5/2}$	$^{18}O_{7.62}(1^-)$	0.300
$^{17}O_{0.87}(1/2^+)$	$1d_{5/2}$	$^{18}O_{5.38}(3^+)$	0.944	$^{17}O_{3.84}(5/2^-)$	$2s_{1/2}$	$^{18}O_{7.77}(2^-)$	−0.086
	$1p_{1/2}$	$^{18}O_{6.20}(1^-)$	−0.111		$1d_{5/2}$		−0.202
	$1p_{1/2}$	$^{18}O_{7.62}(1^-)$	0.026		$1d_{5/2}$	$^{18}O_{7.87}(5^-)$	0.461
	$1d_{5/2}$	$^{18}O_{7.98}(3^+)$	0.203		$1p_{1/2}$	$^{18}O_{7.98}(3^+)$	−0.106
	$1p_{1/2}$	$^{18}O_{8.04}(1^-)$	0.307		$1d_{5/2}$	$^{18}O_{8.04}(1^-)$	−0.438
	$1p_{1/2}$	$^{18}O_{9.00}(1^-)$	0.076		$1d_{5/2}$	$^{18}O_{8.13}(5^-)$	0.449
	$1p_{1/2}$	$^{18}O_{9.10}(1^-)$	0.060		$1p_{1/2}$	$^{18}O_{8.21}(2^+)$	−0.414
	$1p_{1/2}$	$^{18}O_{9.27}(1^-)$	0.067		$2s_{1/2}$	$^{18}O_{8.28}(3^-)$	−0.668
	$1d_{5/2}$	$^{17}O_{g.s.}(5/2^+)$	0.972		$1d_{5/2}$		0.453
$^{16}O_{g.s.}(0^+)$	$2s_{1/2}$	$^{17}O_{0.87}(1/2^+)$	0.975		$2s_{1/2}$	$^{18}O_{8.41}(2^-)$	0.086
	$1p_{1/2}$	$^{17}O_{3.06}(1/2^-)$	−0.291		$1d_{5/2}$		0.102
	$1p_{1/2}$	$^{17}O_{g.s.}(5/2^+)$	−0.719		$1d_{5/2}$	$^{18}O_{9.00}(1^-)$	0.063
$^{16}O_{6.13}(3^-)$	$1d_{5/2}$	$^{17}O_{3.06}(1/2^-)$	−0.605		$1d_{5/2}$	$^{18}O_{9.10}(1^-)$	−0.107
	$2s_{1/2}$	$^{17}O_{3.84}(5/2^-)$	−0.588		$1d_{5/2}$	$^{18}O_{9.27}(1^-)$	0.035
	$1d_{5/2}$		−0.718		$2s_{1/2}$	$^{18}O_{9.36}(3^-)$	−0.019
					$1d_{5/2}$		−0.372

set to equal 1.2 fm and 0.6 fm for ^{16}O and 1.26 fm and 0.80 fm for ^{18}O, respectively as in Refs. [9,13].

Couplings allowed by angular momentum and parity conservation, used in the EFR-CRC and two-step DWBA calculations, are shown in Figs. 3 and 4, for the $^{16}O(t,p)^{18}O$ and $^{16}O(^{18}O,^{16}O)^{18}O$ reactions. Target overlaps are the same for the (t,p) and $(^{18}O,^{16}O)$ reactions. Projectile overlaps are not shown for the (t,p) reaction since we do not consider

TABLE II. Two-neutron spectroscopic amplitudes (SA) for CRC calculations obtained by shell model calculations with ZBM interaction. $n_1 l_{1\,j_1}$ and $n_2 l_{2\,j_2}$ are the principal quantum numbers, the orbital and the total angular momenta of neutrons 1 and 2 with respect to the core; J_{12} is the angular momentum of the two-neutron system.

Initial state	$n_1 l_{1\,j_1}\ n_2 l_{2\,j_2}$	J_{12}	Final state	SA	Initial state	$n_1 l_{1\,j_1}\ n_2 l_{2\,j_2}$	J_{12}	Final state	SA
$^{18}O_{g.s.}(0^+)$	$(1p_{1/2})^2$	0		0.241	$^{18}O_{g.s.}(0^+)$	$1p_{1/2}1d_{5/2}$	3		0.801
	$(1d_{5/2})^2$			−0.871	$^{18}O_{1.98}(2^+)$	$1p_{1/2}1d_{5/2}$	3		0.639
	$(2s_{1/2})^2$			−0.367	$^{18}O_{3.55}(4^+)$	$1p_{1/2}1d_{5/2}$	3		0.733
$^{18}O_{1.98}(2^+)$	$(1d_{5/2})^2$	2		−0.641	$^{18}O_{3.63}(0^+)$	$1p_{1/2}1d_{5/2}$	3		0.338
	$1d_{5/2}2s_{1/2}$			−0.638	$^{18}O_{3.92}(2^+)$	$1p_{1/2}1d_{5/2}$	3		0.683
$^{18}O_{3.55}(4^+)$	$(1d_{5/2})^2$	4		−0.948	$^{18}O_{4.46}(1^-)$	$(1d_{5/2})^2$	2		0.338
$^{18}O_{3.63}(0^+)$	$(1p_{1/2})^2$	0		0.009		$1d_{5/2}2s_{1/2}$			0.376
	$(1d_{5/2})^2$			−0.428	$^{18}O_{5.10}(3^-)$	$(1p_{1/2})^2$	0		−0.198
	$(2s_{1/2})^2$			0.386		$(1d_{5/2})^2$			−0.668
$^{18}O_{3.92}(2^+)$	$(1d_{5/2})^2$	2		−0.686		$(2s_{1/2})^2$			0.371
	$1d_{5/2}2s_{1/2}$			0.597	$^{18}O_{5.25}(2^+)$	$1p_{1/2}2s_{1/2}$	1		−0.198
$^{18}O_{4.46}(1^-)$	$1p_{1/2}2s_{1/2}$	1		−0.079	$^{18}O_{5.34}(0^+)$	$1p_{1/2}1d_{5/2}$	3		−0.180
$^{18}O_{5.10}(3^-)$	$1p_{1/2}1d_{5/2}$	3		0.066	$^{18}O_{5.38}(3^+)$	$1p_{1/2}2s_{1/2}$	1		0.506
$^{18}O_{5.25}(2^+)$	$(1d_{5/2})^2$	0		0.044	$^{18}O_{5.53}(2^-)$	$(1d_{5/2})^2$	2		0.737
	$1d_{5/2}2s_{1/2}$			0.388		$1d_{5/2}2s_{1/2}$			0.491
$^{18}O_{5.34}(0^+)$	$(1p_{1/2})^2$	0		0.010	$^{18}O_{6.20}(1^-)$	$(1d_{5/2})^2$	4		−0.520
	$(1d_{5/2})^2$		$^{16}O_{g.s.}(0^+)$	0.149	$^{18}O_{6.35}(2^-)$	$(1d_{5/2})^2$	2		0.242
	$(2s_{1/2})^2$			−0.798		$1d_{5/2}2s_{1/2}$			0.128
$^{18}O_{5.38}(3^+)$	$1d_{5/2}2s_{1/2}$	3		0.914	$^{18}O_{6.40}(3^-)$	$(1d_{5/2})^2$	2		−0.573
$^{18}O_{5.53}(2^-)$	$1p_{1/2}1d_{5/2}$	2		−0.066		$1d_{5/2}2s_{1/2}$			−0.190
$^{18}O_{6.20}(1^-)$	$1p_{1/2}2s_{1/2}$	1		0.066	$^{18}O_{7.12}(4^+)$	$1p_{1/2}1d_{5/2}$	3	$^{16}O_{6.13}(3^-)$	−0.065
$^{18}O_{6.35}(2^-)$	$1p_{1/2}1d_{5/2}$	2		0.129	$^{18}O_{7.62}(1^-)$	$(1d_{5/2})^2$	2		0.204
$^{18}O_{6.40}(3^-)$	$1p_{1/2}1d_{5/2}$	3		−0.269		$1d_{5/2}2s_{1/2}$			0.222
$^{18}O_{7.12}(4^+)$	$(1d_{5/2})^2$	4		0.002	$^{18}O_{7.77}(2^-)$	$(1d_{5/2})^2$	4		0.513
$^{18}O_{7.62}(1^-)$	$1p_{1/2}2s_{1/2}$	1		0.020	$^{18}O_{7.87}(5^-)$	$(1d_{5/2})^2$	4		−1.032
$^{18}O_{7.77}(2^-)$	$1p_{1/2}1d_{5/2}$	2		0.192	$^{18}O_{7.98}(3^+)$	$1d_{5/2}2s_{1/2}$	1		0.173
$^{18}O_{7.98}(3^+)$	$1d_{5/2}2s_{1/2}$	3		0.289	$^{18}O_{8.04}(1^-)$	$(1d_{5/2})^2$	2		−0.096
$^{18}O_{8.04}(1^-)$	$1p_{1/2}2s_{1/2}$	1		0.272		$1d_{5/2}2s_{1/2}$			0.600
$^{18}O_{8.21}(2^+)$	$(1d_{5/2})^2$	2		0.010	$^{18}O_{8.13}(5^-)$	$(1d_{5/2})^2$	2		−0.180
	$1d_{5/2}2s_{1/2}$			−0.009		$1d_{5/2}2s_{1/2}$			−0.510
$^{18}O_{8.28}(3^-)$	$1p_{1/2}1d_{5/2}$	3		−0.031	$^{18}O_{8.21}(2^+)$	$1p_{1/2}1d_{5/2}$	3		−0.209
$^{18}O_{8.41}(2^-)$	$1p_{1/2}1d_{5/2}$	2		0.078	$^{18}O_{8.28}(3^-)$	$(1p_{1/2})^2$	0		0.027
$^{18}O_{9.00}(1^-)$	$1p_{1/2}2s_{1/2}$	1		0.066		$(1d_{5/2})^2$			0.339
$^{18}O_{9.10}(1^-)$	$1p_{1/2}2s_{1/2}$	1		0.062		$(2s_{1/2})^2$			−0.428
$^{18}O_{9.27}(1^-)$	$1p_{1/2}2s_{1/2}$	1		0.060	$^{18}O_{8.41}(2^-)$	$(1d_{5/2})^2$	2		0.388
$^{18}O_{9.36}(3^-)$	$1p_{1/2}1d_{5/2}$	3		0.028		$1d_{5/2}2s_{1/2}$			−0.117
					$^{18}O_{9.00}(1^-)$	$(1d_{5/2})^2$	4		−0.535
					$^{18}O_{9.00}(1^-)$	$(1d_{5/2})^2$	2		0.071
						$1d_{5/2}2s_{1/2}$			−0.135
					$^{18}O_{9.27}(1^-)$	$(1d_{5/2})^2$	2		0.065
						$1d_{5/2}2s_{1/2}$			0.270
						$(1p_{1/2})^2$			−0.061
					$^{18}O_{9.36}(3^-)$	$(1d_{5/2})^2$	0		0.144
						$(2s_{1/2})^2$			−0.050

any unbound state of the triton and deuteron, focusing on the couplings to the ground states. For the (^{18}O,^{16}O) reaction, the projectile and target overlaps in the entrance partition refer to the 0_1^+(g.s.), 2_1^+(1.98 MeV), and 4_1^+ (3.55 MeV) states of ^{18}O and 0_1^+(g.s.) and 3_1^- (6.23 MeV) states of ^{16}O.

B. Spectroscopic amplitudes

Spectroscopic amplitudes in the extreme cluster model are set equal to 1.0 for all the couplings. The two-neutron system can be modeled in a singlet ($S = 0$) or triplet state ($S = 1$). The effect of the two-neutron configuration has been

already observed for the ^{16}O(^{18}O,^{16}O)^{18}O reaction leading to the 0^+_1 and 2^+_1 states [13]. Within the scope of the extreme cluster model and due to parity conservation, the natural parity states of the ^{18}O nucleus are mainly populated by the singlet two-neutron state, the triplet one being the only possible configuration for unnatural parity states. Therefore, we adopt the pure singlet two-neutron state whenever parity conservation allows it and the pure triplet state otherwise.

In the independent coordinates model and two-step DWBA calculations, we used spectroscopic amplitudes derived from shell model calculations with the Zuker-Buck-McGrory (ZBM) interaction, which is an effective interaction for the $1p_{1/2}$, $2s_{1/2}$, and $1d_{5/2}$ orbitals [22]. This valence space has the advantage that most of states at the *p-sd* interface around ^{16}O are described through configuration mixing of these three orbitals. In the model space, a ^{12}C core was considered, which is suitable to describe the nuclear structure of the ^{16,17,18}O isotopes [9,13]. The excitation energy spectra populated by the ^{16}O$(d,p)^{17}$O reaction have been reported in [23], in which a peak is observed at $\sim$5.08 MeV, corresponding to the $3/2^+$ state. In this way, an accurate description of the high-lying states ($\gtrsim$5 MeV) in the ^{18}O nucleus possibly requires the $1d_{3/2}$ and $1f_{7/2}$ orbitals, and the inclusion of these orbitals requires a proper interaction not available at this moment. Despite the expected relevance of the $1d_{3/2}$ orbital, the good agreement observed in the (t,p) data (shown in Sec. IV A) with the chosen model space seems to indicate that the omitted orbitals do not appreciably affect our comparisons.

The spectroscopic amplitudes for one- and two-neutron transfers in the ^{16}O$(t,p)^{18}$O reaction are listed in Tables I and II, respectively. For the ^{16}O(^{18}O,^{16}O)^{18}O reaction, the spectroscopic amplitudes are the same as in Tables I and II; just the initial and final states will be interchanged. We have taken all the experimentally available states up to 9.36 MeV (3^+), except the 8.52, 8.66, 8.82, 8.96, and 9.03 MeV states, for which there is not a clear assignment of the spins and parities. For the 9.1 and 9.27 MeV excited states, we have considered the 1^-. It must be highlighted that the spectroscopic amplitudes derived for the first three 0^+ states (the ground, 3.63 MeV, and 5.34 MeV states) are very close to the values independently deduced in Ref. [1]. For the 0^+_3, for instance, the spectroscopic amplitudes for the $(1d_{5/2})^2$ and the $(2s_{1/2})^2$ components are 0.229 and -0.870 (from Ref. [1]) and 0.149 and -0.798 (see Table II), respectively.

IV. DISCUSSIONS

A. Angular distributions for the ^{16}O$(t,p)^{18}$O reaction

Experimental data and calculations for the population of 15 states of ^{18}O are shown in Fig. 5. The solid, dotted, and dashed lines correspond to the results of the independent coordinates (IC), cluster (Clust) and sequential transfer (two-step DWBA) models, respectively.

The overall magnitude of the cross sections for the 0^+_1 ground state is reasonably well described by the IC approach, although the oscillations observed in the experimental data points are better reproduced by the cluster model. An even better agreement is achieved when the strength coefficient for the imaginary part of the optical potential is reduced, since many channels are explicitly included in the calculations. Experimental data for the elastic scattering of ^{18}O + ^{16}O, which is not available in the literature, would allow for a better determination of the parameters of the optical potential. Nevertheless, reducing imaginary strength of the optical potential does not change the importance of simultaneous transfer over sequential transfer. In order to establish a unique description for both (t,p) and (^{18}O,^{16}O) reactions, the 0.6 strength factor is considered throughout this work, as already mentioned in Sec. III A. The shape, order, and local minima for the angular distributions of the 2^+_1 (1.98 MeV) and 4^+_1 (3.55 MeV) states are almost equally well described by the cluster and IC calculations. For the 0^+_2 (3.63 MeV) and 2^+_2 (3.92 MeV) we observe a competition between the simultaneous and sequential processes, according to our calculations. For the 1^-_1 (4.46 MeV), 3^-_1 (5.10 MeV), and 2^+_3 coherent (5.25 MeV) states, once again the IC calculation reproduces better the experimental data, while the two-step DWBA cross sections are quite small for the negative-parity states. So far, we notice the predominance of the simultaneous two-neutron transfer process for the population of natural parity final states.

The 3^+_1 (5.38 MeV) state is the first unnatural parity state in the ^{18}O energy spectra. Within the scope of the extreme cluster model, this state is allowed to be populated only by a triplet ($S = 1$) two-neutron system. The same limitation applies to the 2^-_1 (5.53 MeV) and 2^-_2 (6.35 MeV) states. For the 3^+_1 state, the two-step DWBA reproduces fairly well the experimental data, and the sequential two-neutron transfer is the most important process (see in Fig. 5). For the 2^- states, calculations tend to underestimate the cross sections. This feature seems to arise from the limitations imposed in our model space for the shell model calculations, mainly above $\sim$5 MeV, where the $1d_{3/2}$ and $1f_{7/2}$ orbits could also contribute. That might also affect the results observed for the 1^-_2 (6.20 MeV) state, for which the experimental data lie between the IC and the cluster curves. However, the cluster model produces a reasonably good agreement with the experimental data for the 4^+_2(7.12 MeV) state while the IC model and two-step DWBA lie more than one order of magnitude lower.

B. Angular distributions for the ^{16}O(^{18}O,^{16}O)^{18}O reaction

The experimental angular distributions for the natural parity states 0^+_1, 2^+_1, 1^-_1, and 4^+_2 are shown in Fig. 6 along with the theoretical curves. From our calculations we observe the dominance of simultaneous transfer in all natural parity states. We point out two differences in the present calculations. First, the number of couplings included here is larger than in the previous work [13]. We also have included the 3^-_1 (6.13 MeV) state of ^{16}O and the 4^+_1 state of ^{18}O that are used in the couplings of the entrance partition (see Tables I and II). Second, we have used the *s*, *p*, and *d* relative angular momenta of the two transferred neutrons in the IC model. In our previous work we considered the *s* transfer only. In the present work, the inclusion of the *p* and *d* angular momenta slightly improves the agreement with the experimental data for the 0^+_1 and 2^+_1

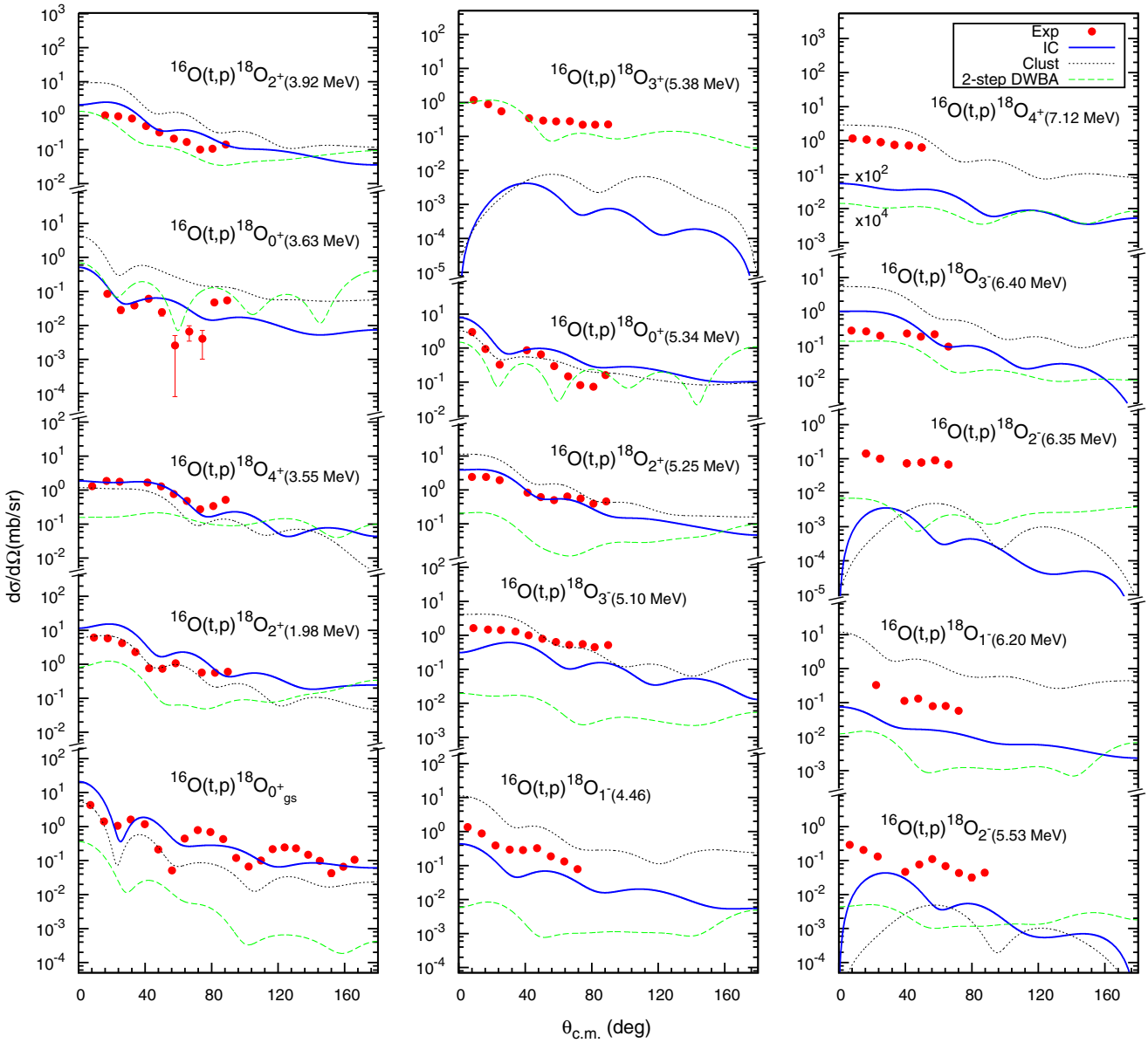

FIG. 5. Comparison of angular distributions of the $^{16}O(t,p)^{18}O$ data and the calculations obtained within the independent coordinates (IC), extreme cluster (Clust), and two-step DWBA approaches.

states (see Fig. 6). Nevertheless, this fact does not change the conclusions established in the previous work.

For the 1^-_1 state, theoretical calculations do not reproduce the absolute cross sections of the data points. The IC and the extreme cluster models seem to establish a lower and an upper limit for the cross sections. A similar result is observed in the population of this state in the (t,p) reaction. We only speculate that such a state can be sensitive to the inelastic channels couplings and/or the truncation of the model space adopted for the calculations of the spectroscopic amplitudes.

The extreme cluster model produces a reasonably good agreement for the 4^+_2 state. Such a state (at 7.12 MeV) is close to the one-neutron threshold (8.05 MeV). The spectroscopic amplitude for this state may be affected by the absence of the $1d_{3/2}$ orbital in our model space. Nevertheless, the model indeed provides good predictions for the absolute cross sections in the (t,p) and the $(^{18}O,^{16}O)$ reactions. This is an indication that the two-neutron system is still strongly correlated in the 4^+_2 state. This behavior resembles the one observed for the 4^+ state at 10.74 MeV populated in $^{12}C(^{18}O,^{16}O)^{14}C$ [9].

In Fig. 7, we show the experimental and theoretical results for the groups of unresolved states: (a) $4^+_1+0^+_2+2^+_2$, (b) $3^-_1+2^+_3+0^+_3+3^+_1$, (c) $3^+_2+1^-_3+5^-_1+2^+_4+3^-_3$ (at 7.98, 8.04, 8.13, 8.21, and 8.28 MeV excitation energies, respectively), and (d) the resonant structure at ∼9.10 MeV which, in this work, is treated as a composition of the 9.00, 9.10, 9.26, and 9.36 MeV states. Angular distributions exhibited in Fig. 7 correspond to the sum of all states within the unresolved group and for each model (cluster, IC, and two-step DWBA).

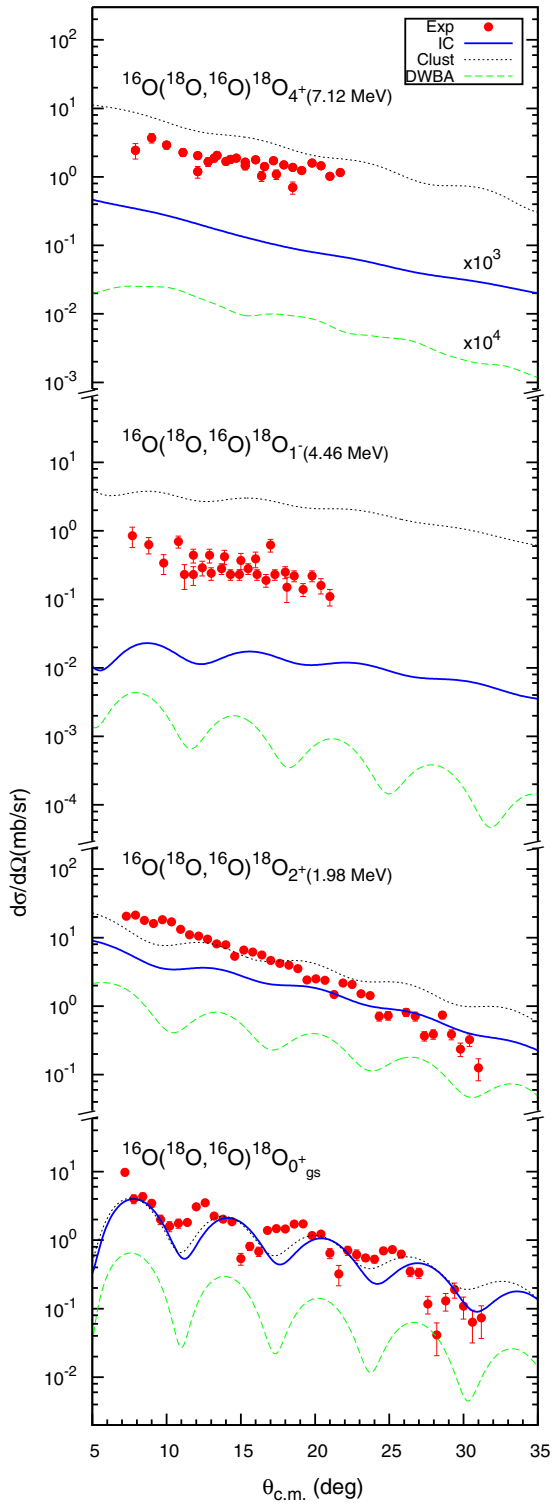

FIG. 6. Comparison of angular distributions of the ^{16}O(^{18}O,^{16}O)^{18}O data and the calculations obtained within the independent coordinates (IC), extreme cluster (Clust), and two-step DWBA approaches.

A common feature observed is the weak contribution from sequential transfer in the explored energy window. This property, also observed in (t,p), is a consequence of the selectivity of these reactions to natural parity states. For these

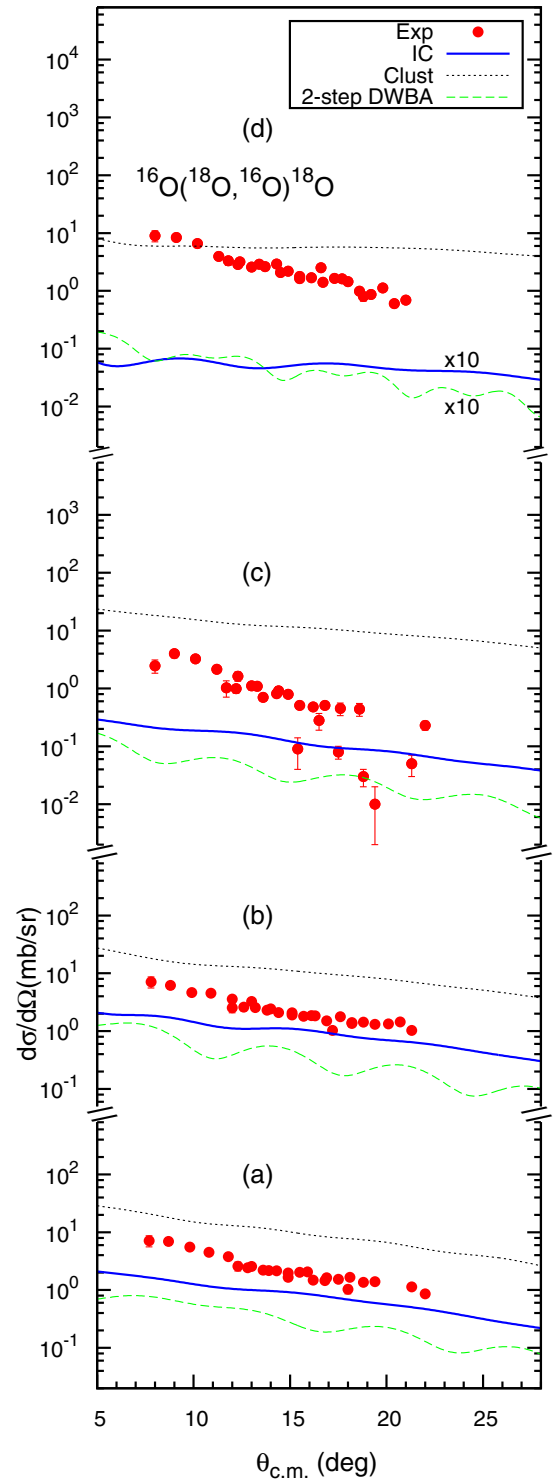

FIG. 7. Comparison of sum of the angular distributions of the: (a) 4^+(3.55 MeV), 0^+(3.63 MeV) and 2^+(3.92 MeV); (b) 3^-(5.10 MeV), 2^+(5.25) MeV, 0^+(5.34 MeV), 3^+(5.38 MeV) and 2^-(5.53 MeV); (c) 3^+(7.99 MeV), 1^-(8.04 MeV) and 3^-(8.28 MeV); (d) 1^- (9.00 MeV), 1^- (9.10 MeV), 1^- (9.28 MeV) and 3^- (9.36 MeV) states of ^{18}O obtained within independent coordinates (IC), cluster(Clust) and the two-step DWBA schemes with the experimental data on ^{16}O(^{18}O,^{16}O)^{18}O reaction.

latter, the role of antiparallel neutron-neutron configuration is dominant due to the relevant pairing interaction in this channel.

The first unresolved group of states ($4^+_1 + 0^+_2 + 2^+_2$) is composed of natural parity states that are reasonably well described by the IC model in the ^{16}O$(t,p)^{18}$O reaction (see Fig. 5). For the ^{16}O(^{18}O,^{16}O)^{18}O reaction, the cluster and IC calculations reproduce the overall shape of the experimental data, but the cluster model overestimates and the IC model underestimates the absolute cross sections.

The next group of states ($3^-_1 + 2^+_3 + 0^+_3 + 3^+_1$) contains an unnatural parity state (3^+_1). For this particular state, the sequential transfer shall be the most relevant process, as observed in the analysis of the ^{16}O$(t,p)^{18}$O. However, the experimental data lie between the IC and the two-step DWBA curves. The same feature is exhibited in the third group of states ($3^+_2 + 1^-_3 + 5^-_1 + 2^+_4 + 3^-_3$), which contains also another unnatural parity state (3^+_2).

For the resonant structure at ∼9.10 MeV, we have considered contributions from negative parity states, accordingly to the NNDC database [24] and also observed in the (t,p) experiment [14]. From the shell model results, possible I^π assignment for the first three states (9.00, 9.10, and 9.26 MeV) are $I^\pi = 0^-$, 1^-, or 2^-. Among these possibilities, the 1^- is the one that produces absolute cross sections of the order of magnitude observed in the experimental data. In Fig. 7(d), we show these results assuming $I^\pi = 1^-$ for the 9.00, 9.10, and 9.26 MeV states and 3^- for the 9.36 MeV state. The extreme cluster model does not describe the shape observed in the experimental data. We have performed calculations for the sequential process (not shown here) considering different I^π assignments. All of these calculations indicate very small changes.

V. SUMMARY

In this work we revisit the two-neutron transfer in the ^{16}O$(t,p)^{16}$O and ^{16}O(^{18}O,^{16}O)^{18}O reactions. We provide new experimental data for the high-lying ^{18}O states populated in the ^{16}O(^{18}O,^{16}O)^{18}O reaction. The experimental angular distributions are analyzed within a theoretical formalism in which the sequential two-neutron transfer is calculated within the two-step DWBA and the simultaneous processes are calculated in the EFR-CRC, considering the two-neutron system within the extreme cluster and the independent coordinates approaches. The spectroscopic amplitudes are derived independently, within the shell model formalism in which the ZBM interaction is adopted.

Here we show that accurate direct reaction calculations, with a no-free parameter approach, are able to reproduce the experimental data for the natural parity ^{18}O states populated in the (t,p) and in the (^{18}O,^{16}O) reactions. The consistency of our results establishes a close relationship between the two-neutron transfer processes in these two different reactions. Spectroscopic studies with transfer reactions induced by heavy ions are feasible for the natural parity states, although some limitations still remain for the unnatural ones. We conclude that the one-step simultaneous transfer of the two neutrons is an important mechanism for the population of natural parity states of ^{18}O both in (t,p) and (^{18}O,^{16}O) reactions. We find that both the experiment and the calculations show a large population of natural parity states, indicating an active role in the reaction of the *n*-*n* pairing correlation, present in the triton and ^{18}O$_{\text{g.s.}}$ wave functions. The extreme cluster model tends to overestimate the data as a consequence of the assumed amplitude of the cluster configurations. However, a possible scaling of the cluster calculations to the data would indicate a sizable cluster component in the wave functions of the populated states. In particular, the fairly good agreement of the cluster model for the high-lying 4^+_2 state is an indication that the two-neutron pairing correlation is important. The IC model, on the other hand, is sensitive to the chosen model space for the shell model amplitudes, resulting in a systematic trend to underestimate the cross sections at high excitation energies.

ACKNOWLEDGMENTS

M.J.E.'s work is supported by a grant from CNPq-Brazil (Process No. 165371/2015-3). J.L., J.L.F., R.L. and V.A.B.Z. acknowledge partial support from CNPq and FAPERJ (Brazil).

[1] H. Fortune and S. Headley, Phys. Lett. B **51**, 136 (1974).
[2] A. Deltuva and A. C. Fonseca, Phys. Rev. C **95**, 024003 (2017).
[3] F. Ajzenberg-Selove, E. R. Flynn, and O. Hansen, Phys. Rev. C **17**, 1283 (1978).
[4] M. Igarashi, K.-i. Kubo, and K. Yagi, Phys. Rep. **199**, 1 (1991).
[5] G. Potel, A. Idini, F. Barranco, E. Vigezzi, and R. A. Broglia, Phys. Rev. C **87**, 054321 (2013).
[6] G. Potel, F. Barranco, F. Marini, A. Idini, E. Vigezzi, and R. A. Broglia, Phys. Rev. Lett. **107**, 092501 (2011).
[7] D. Brink, Phys. Lett. B **40**, 37 (1972).
[8] F. Cappuzzello, C. Rea, A. Bonaccorso, M. Bondì, D. Carbone, M. Cavallaro, A. Cunsolo, A. Foti, S. Orrigo, M. Rodrigues, and G. Taranto, Phys. Lett. B **711**, 347 (2012).
[9] M. Cavallaro, F. Cappuzzello, M. Bondì, D. Carbone, V. N. Garcia, A. Gargano, S. M. Lenzi, J. Lubian, C. Agodi, F. Azaiez, M. De Napoli, A. Foti, S. Franchoo, R. Linares, D. Nicolosi, M. Niikura, J. A. Scarpaci, and S. Tropea, Phys. Rev. C **88**, 054601 (2013).
[10] F. Cappuzzello, D. Carbone, M. Cavallaro, M. Bondì, C. Agodi, F. Azaiez, A. Bonaccorso, A. Cunsolo, L. Fortunato, A. Foti, S. Franchoo, E. Khan, R. Linares, J. Lubian, J. A. Scarpaci, and A. Vitturi, Nat. Commun. **6**, 6743 (2015).
[11] D. Carbone, M. Bondì, A. Bonaccorso, C. Agodi, F. Cappuzzello, M. Cavallaro, R. J. Charity, A. Cunsolo, M. De Napoli, and A. Foti, Phys. Rev. C **90**, 064621 (2014).
[12] D. Carbone, J. L. Ferreira, F. Cappuzzello, J. Lubian, C. Agodi, M. Cavallaro, A. Foti, A. Gargano, S. M. Lenzi, R. Linares, and G. Santagati, Phys. Rev. C **95**, 034603 (2017).
[13] M. J. Ermamatov, F. Cappuzzello, J. Lubian, M. Cubero, C. Agodi, D. Carbone, M. Cavallaro, J. L. Ferreira, A. Foti, V. N. Garcia, A. Gargano, J. A. Lay, S. M. Lenzi, R. Linares, G. Santagati, and A. Vitturi, Phys. Rev. C **94**, 024610 (2016).

[14] M. E. Cobern, L. C. Bland, H. T. Fortune, G. E. Moore, S. Mordechai, and R. Middleton, Phys. Rev. C **23**, 2387 (1981).
[15] F. Cappuzzello, C. Agodi, D. Carbone, and M. Cavallaro, Eur. Phys. J. A **52**, 167 (2016).
[16] M.-C. Lemaire and K. S. Low, Phys. Rev. C **16**, 183 (1977).
[17] M. Moshinsky, Nucl. Phys. **13**, 104 (1959).
[18] L. C. Chamon, B. V. Carlson, L. R. Gasques, D. Pereira, C. De Conti, M. A. G. Alvarez, M. S. Hussein, M. A. Candido Ribeiro, E. S. Rossi, and C. P. Silva, Phys. Rev. C **66**, 014610 (2002).
[19] D. Pereira, J. Lubian, J. Oliveira, D. de Sousa, and L. Chamon, Phys. Lett. B **670**, 330 (2009).
[20] L. Gasques, L. Chamon, P. Gomes, and J. Lubian, Nucl. Phys. A **764**, 135 (2006).
[21] D. Pereira, R. Linares, J. Oliveira, J. Lubian, L. Chamon, P. Gomes, A. Cunsolo, F. Cappuzzello, M. Cavallaro, D. Carbone, and A. Foti, Phys. Lett. B **710**, 426 (2012).
[22] A. P. Zuker, B. Buck, and J. B. McGrory, Phys. Rev. Lett. **21**, 39 (1968).
[23] M. Cooper, W. Hornyak, and P. Roos, Nucl. Phys. A **218**, 249 (1974).
[24] J. Tuli, Nucl. Instrum. Methods Phys. Res., Sect. A **369**, 506 (1996).